

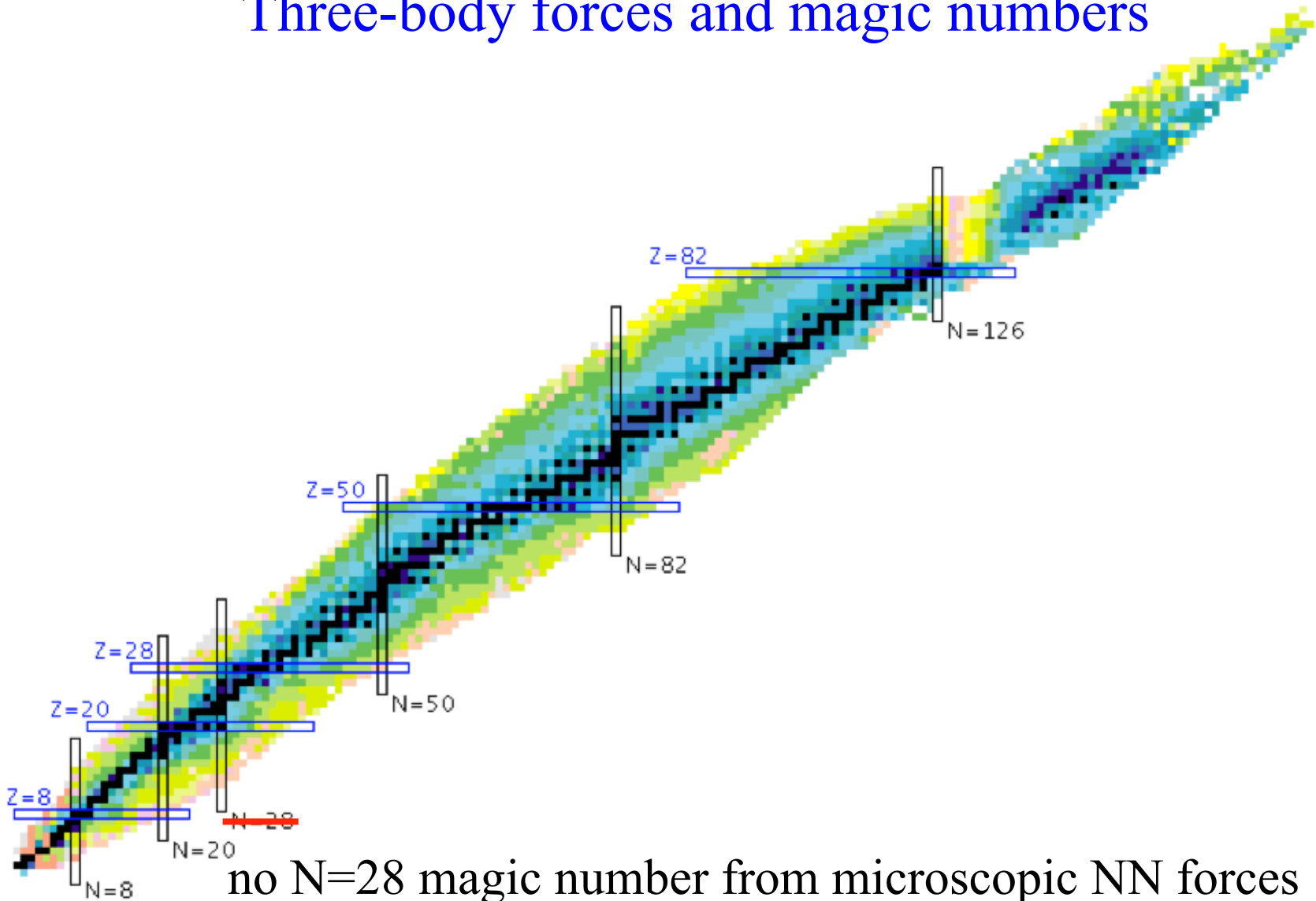
# Outline

3N forces and exotic nuclei

Nuclear physics for direct dark matter detection

Nuclear physics for neutrinoless double-beta decay

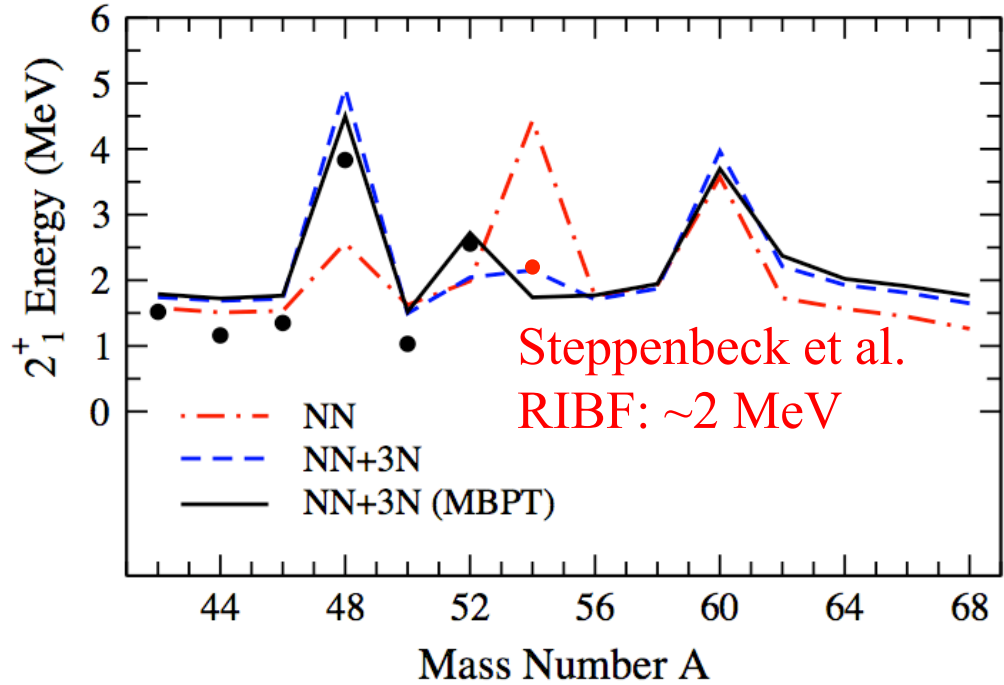
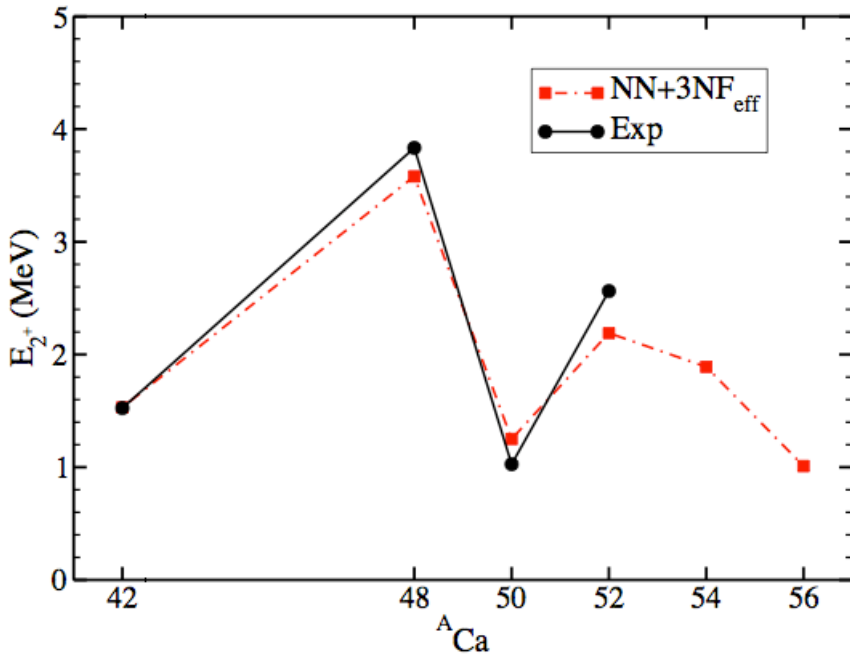
# Three-body forces and magic numbers



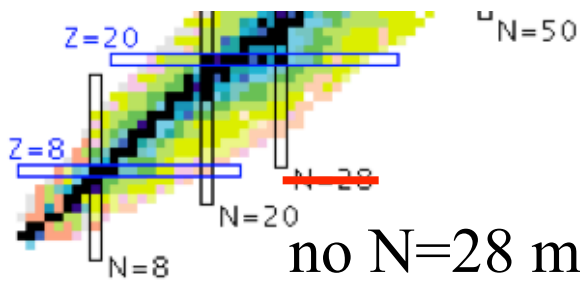
no  $N=28$  magic number from microscopic NN forces

Zuker, Poves,...

# Three-body forces and magic numbers



Hagen et al. (2012)



no N=28 magic number from microscopic NN forces

Zuker, Poves, ...

Holt et al. (2012, 2013)

without 3N forces to 3rd order,  
2<sup>+</sup> is higher in <sup>54</sup>Ca

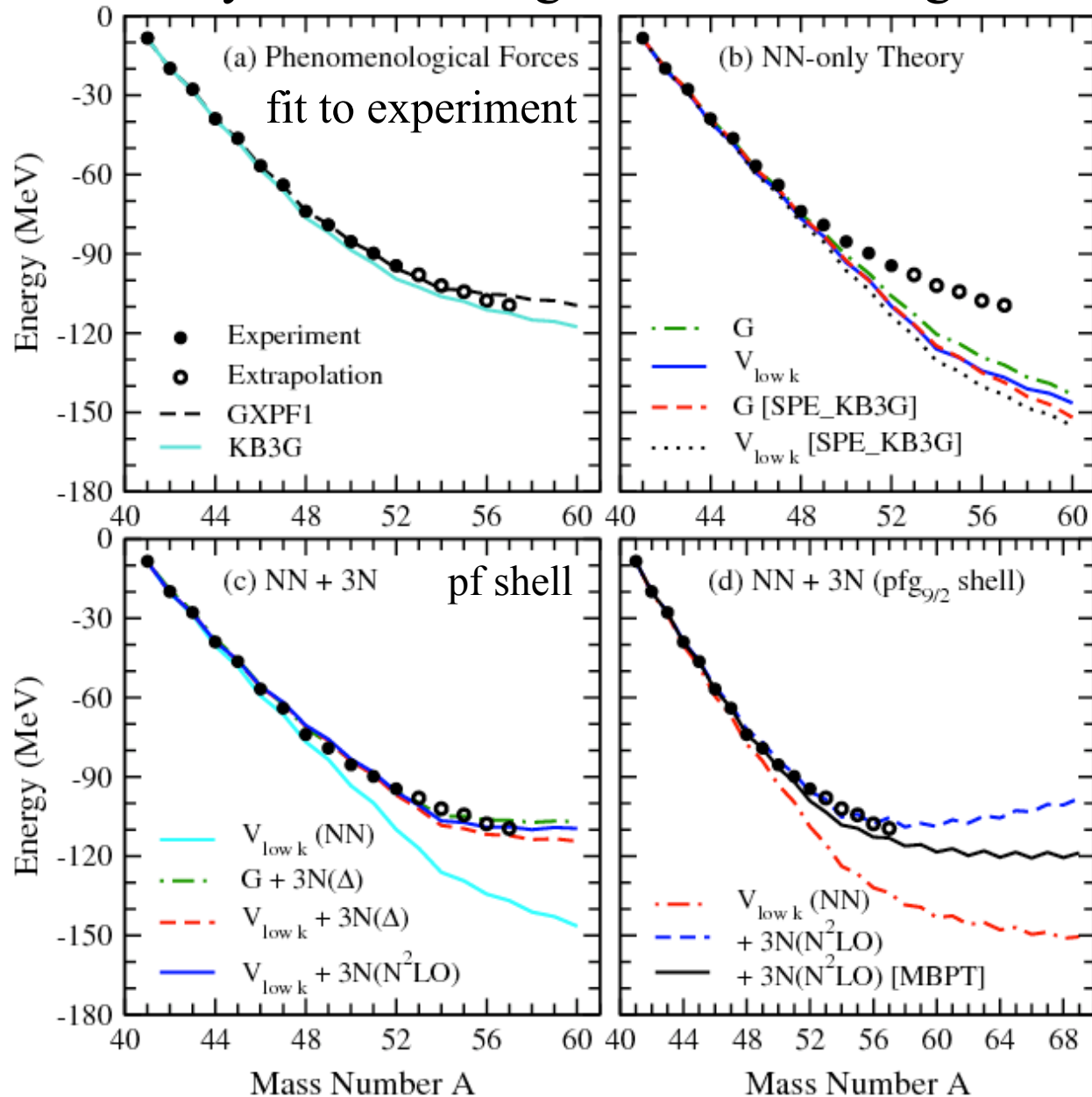
# Evolution to neutron-rich calcium isotopes

repulsive 3N contributions also key for calcium ground-state energies

Holt, Otsuka, AS, Suzuki (2012)

mass measured to  $^{52}\text{Ca}$   
shown to exist to  $^{58}\text{Ca}$

gs energy flat with N,  
continuum important  
for dripline location



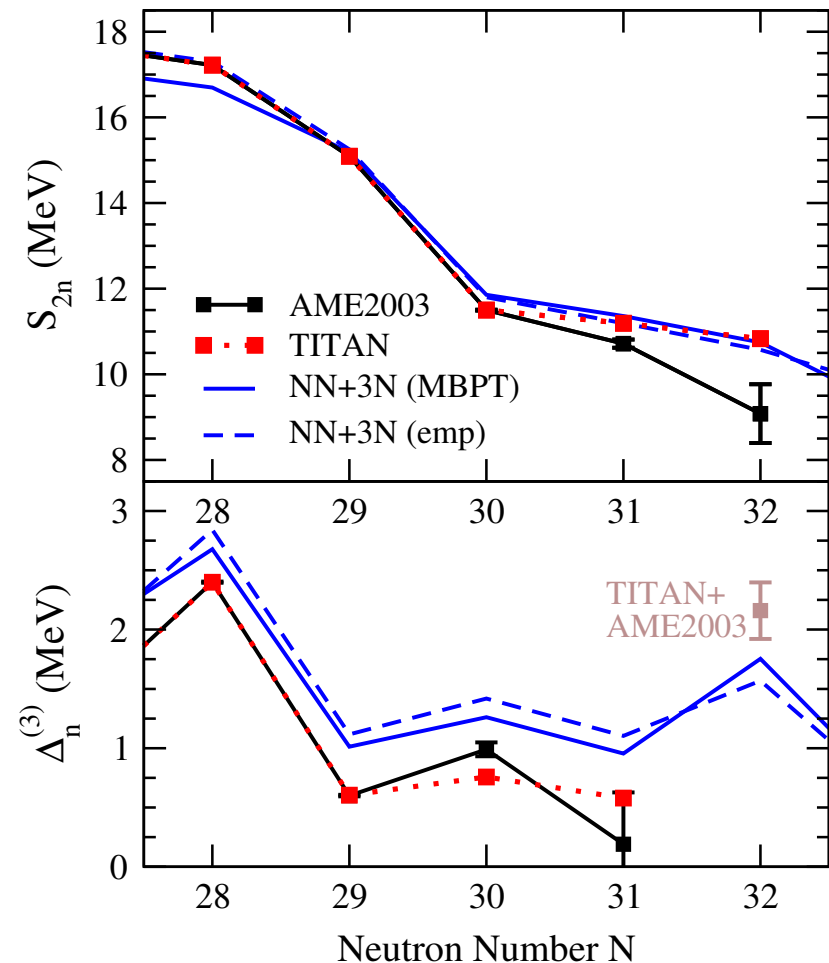
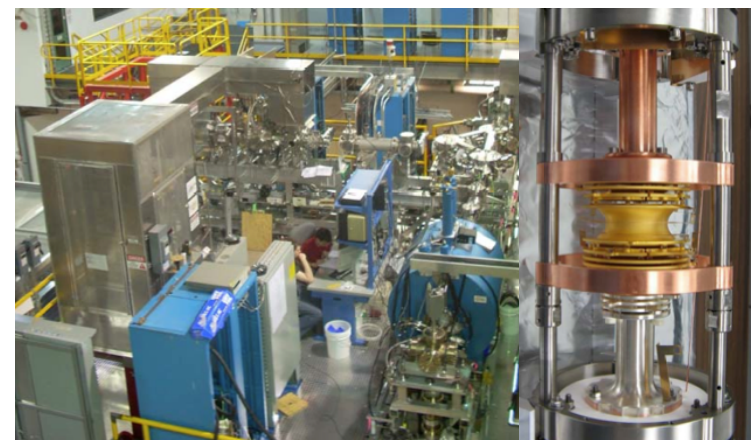


# new $^{51,52}\text{Ca}$ TITAN measurements

$^{52}\text{Ca}$  is 1.75 MeV more bound compared to atomic mass evaluation

Gallant et al. (2012)

behavior of  $2n$  separation energy  $S_{2n}$  agrees with NN+3N predictions



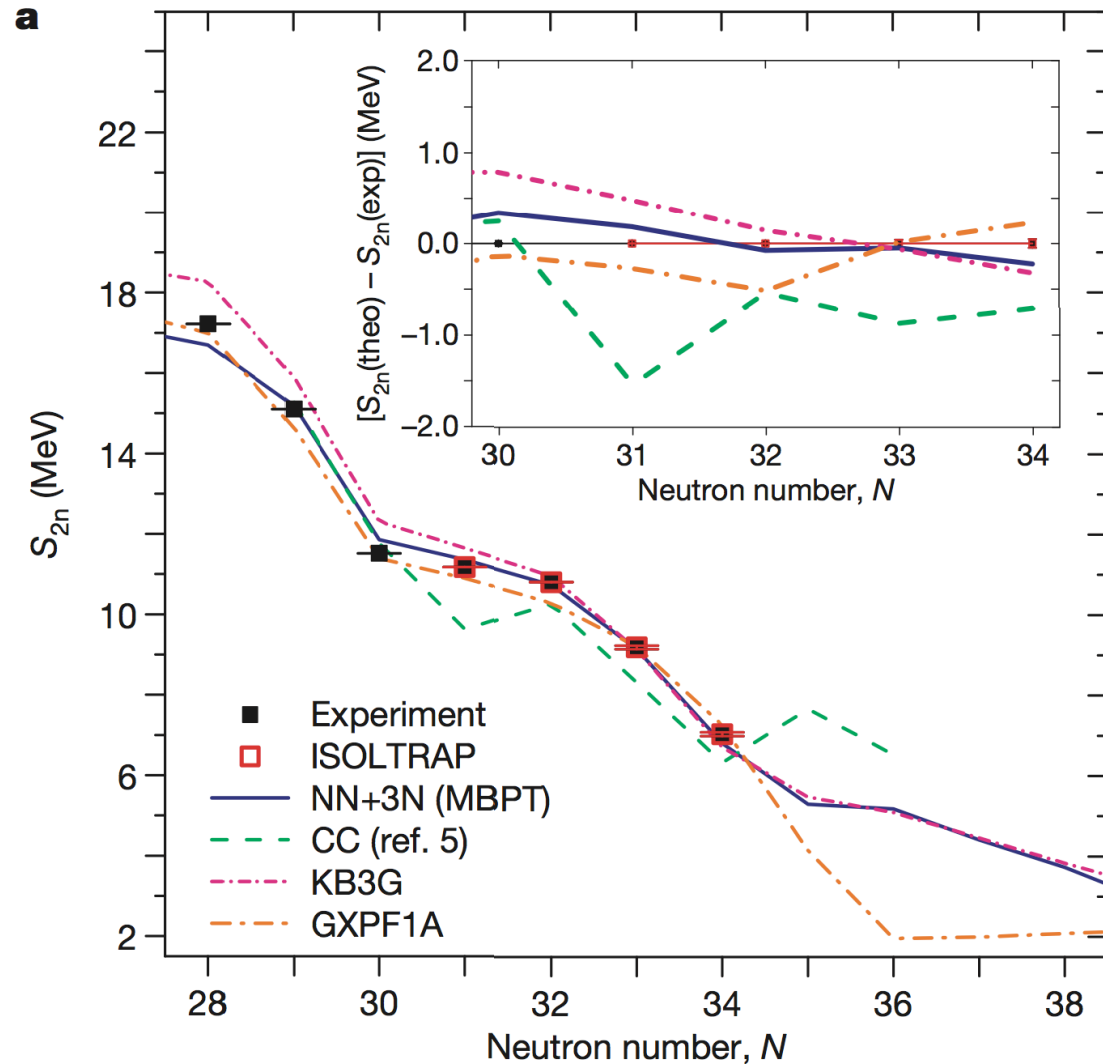
# Masses of exotic calcium isotopes pin down nuclear forces

F. Wienholtz<sup>1</sup>, D. Beck<sup>2</sup>, K. Blaum<sup>3</sup>, Ch. Borgmann<sup>3</sup>, M. Breitenfeldt<sup>4</sup>, R. B. Cakirli<sup>3,5</sup>, S. George<sup>1</sup>, F. Herfurth<sup>2</sup>, J. D. Holt<sup>6,7</sup>, M. Kowalska<sup>8</sup>, S. Kreim<sup>3,8</sup>, D. Lunney<sup>9</sup>, V. Manea<sup>9</sup>, J. Menéndez<sup>6,7</sup>, D. Neidherr<sup>2</sup>, M. Rosenbusch<sup>1</sup>, L. Schweikhard<sup>1</sup>, A. Schwenk<sup>7,6</sup>, J. Simonis<sup>6,7</sup>, J. Stanja<sup>10</sup>, R. N. Wolf<sup>1</sup> & K. Zuber<sup>10</sup>

<sup>53,54</sup>Ca masses measured at ISOLTRAP using new MR-TOF mass spectrometer

establish prominent N=32 shell closure in calcium

excellent agreement with theoretical predictions



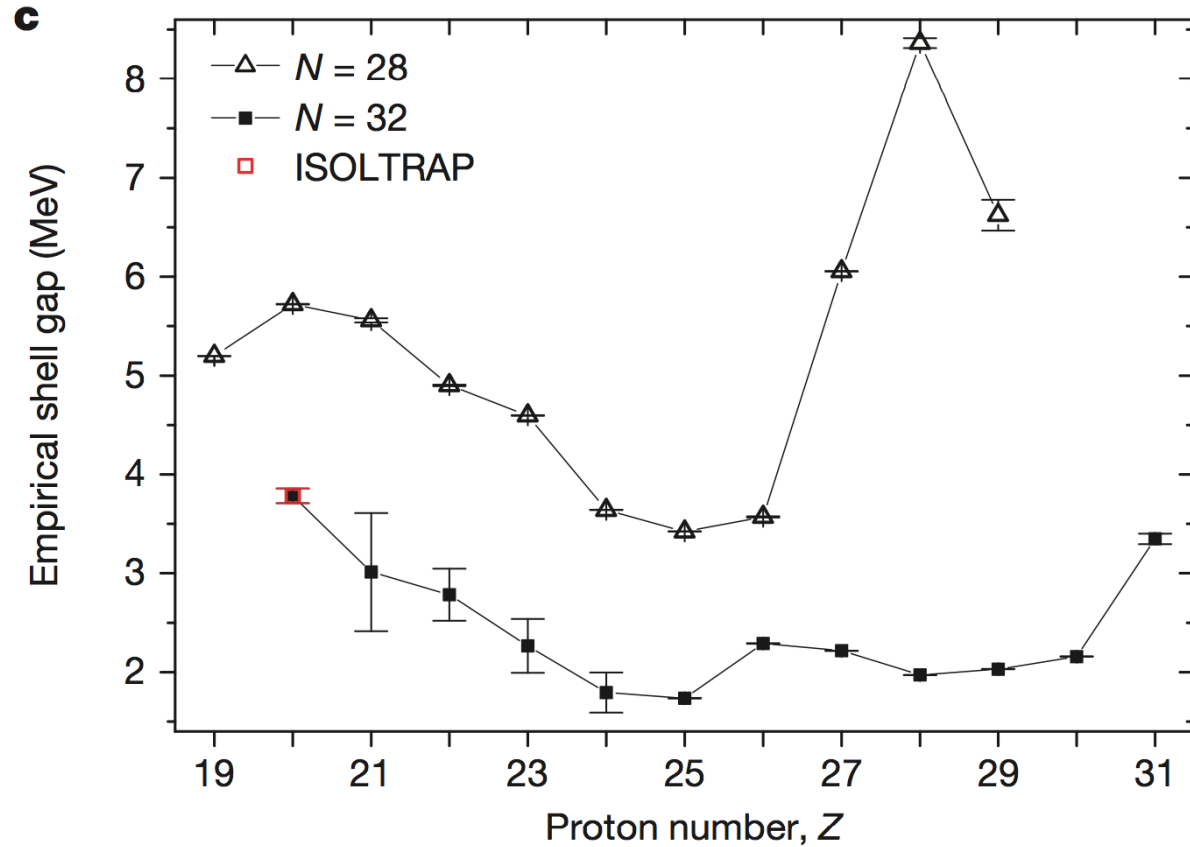
# Masses of exotic calcium isotopes pin down nuclear forces

F. Wienholtz<sup>1</sup>, D. Beck<sup>2</sup>, K. Blaum<sup>3</sup>, Ch. Borgmann<sup>3</sup>, M. Breitenfeldt<sup>4</sup>, R. B. Cakirli<sup>3,5</sup>, S. George<sup>1</sup>, F. Herfurth<sup>2</sup>, J. D. Holt<sup>6,7</sup>, M. Kowalska<sup>8</sup>, S. Kreim<sup>3,8</sup>, D. Lunney<sup>9</sup>, V. Manea<sup>9</sup>, J. Menéndez<sup>6,7</sup>, D. Neidherr<sup>2</sup>, M. Rosenbusch<sup>1</sup>, L. Schweikhard<sup>1</sup>, A. Schwenk<sup>7,6</sup>, J. Simonis<sup>6,7</sup>, J. Stanja<sup>10</sup>, R. N. Wolf<sup>1</sup> & K. Zuber<sup>10</sup>

shell gap of 4 MeV

evolution to  $Z=20$

similar for  $N=28$  and 32



# Masses of exotic calcium isotopes pin down nuclear forces

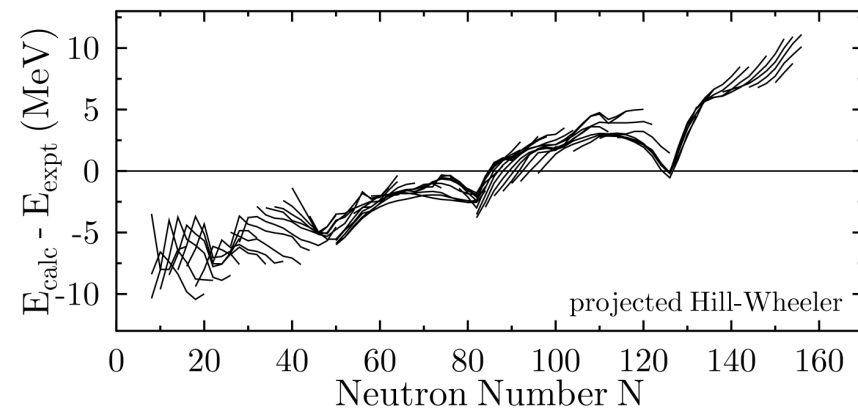
F. Wienholtz<sup>1</sup>, D. Beck<sup>2</sup>, K. Blaum<sup>3</sup>, Ch. Borgmann<sup>3</sup>, M. Breitenfeldt<sup>4</sup>, R. B. Cakirli<sup>3,5</sup>, S. George<sup>1</sup>, F. Herfurth<sup>2</sup>, J. D. Holt<sup>6,7</sup>, M. Kowalska<sup>8</sup>, S. Kreim<sup>3,8</sup>, D. Lunney<sup>9</sup>, V. Manea<sup>9</sup>, J. Menéndez<sup>6,7</sup>, D. Neidherr<sup>2</sup>, M. Rosenbusch<sup>1</sup>, L. Schweikhard<sup>1</sup>, A. Schwenk<sup>7,6</sup>, J. Simonis<sup>6,7</sup>, J. Stanja<sup>10</sup>, R. N. Wolf<sup>1</sup> & K. Zuber<sup>10</sup>

overall good agreement with density functional predictions

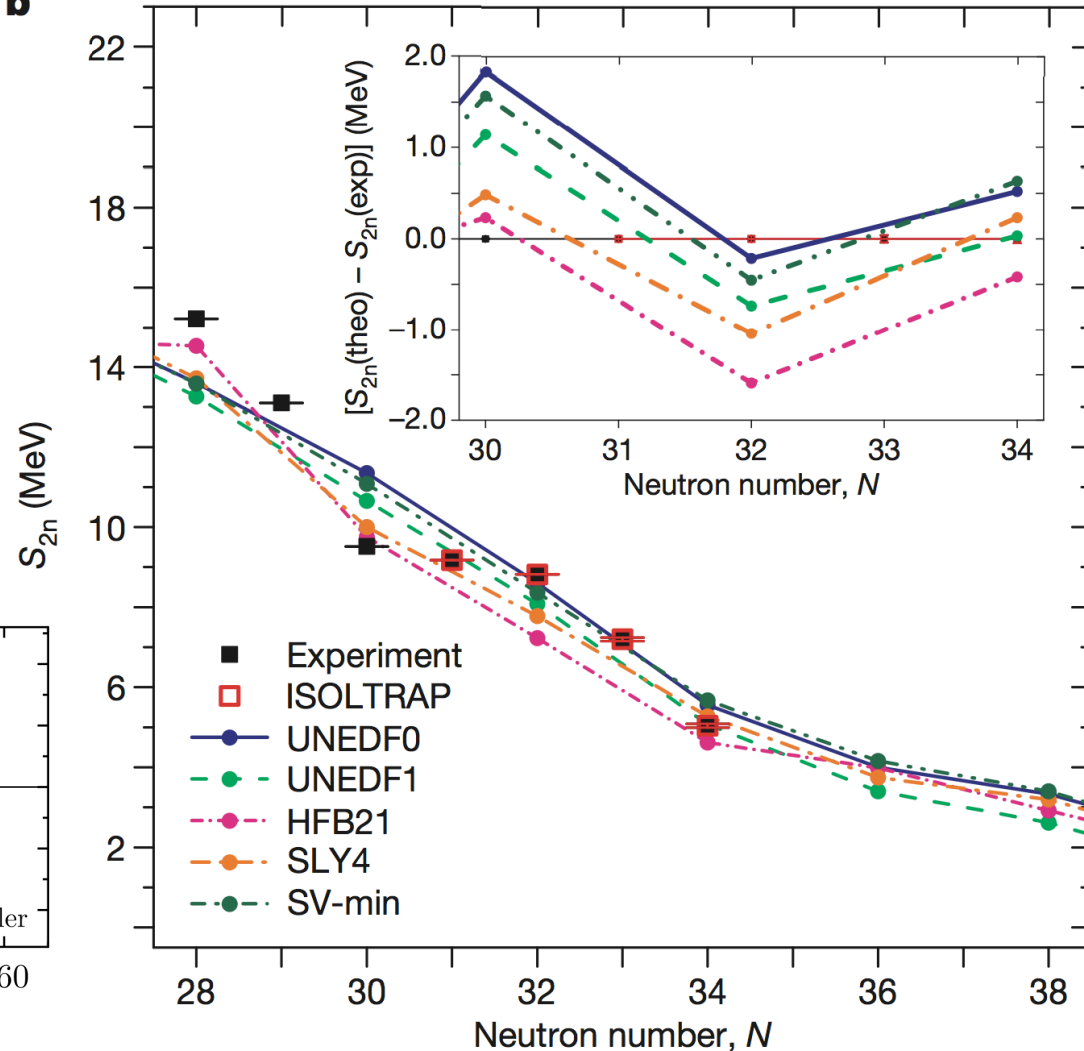
but DF's do not reproduce shell closures

cf. N=50, 82, 126 “arches”

Bender et al. (2005)

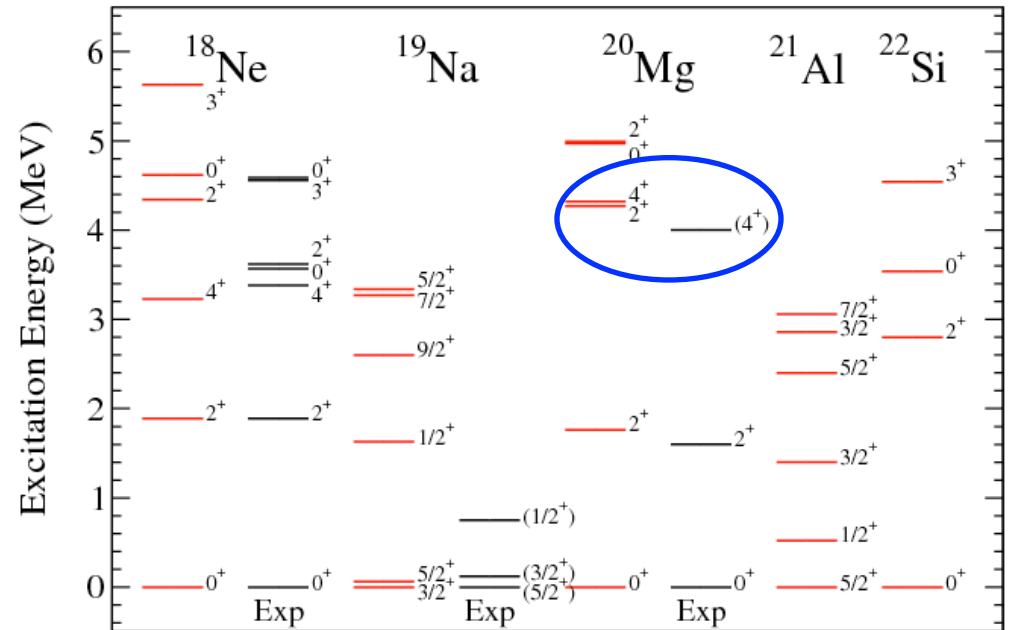
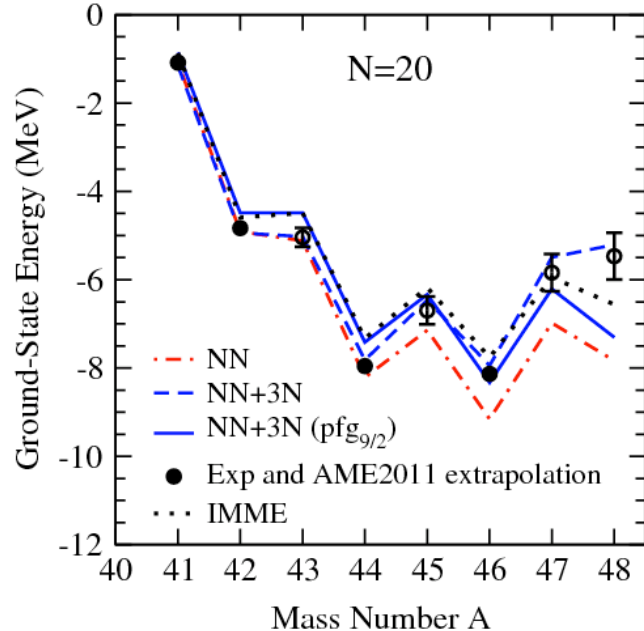
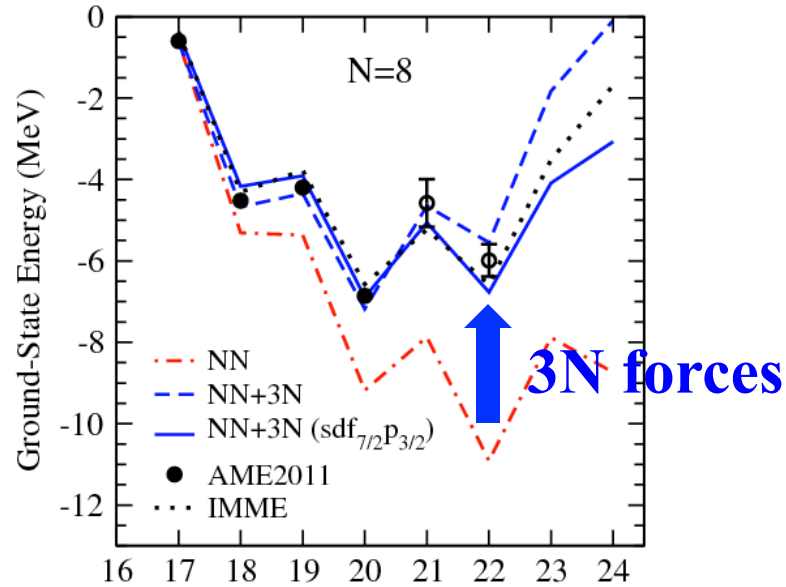


**b**



# 3N forces and proton-rich nuclei Holt, Menendez, AS (2013)

first results with 3N forces for ground and excited states of N=8, 20



prediction for <sup>20</sup>Mg agrees with new state observed at GSI Mukha, private comm.

# Tensor forces and exotic nuclei Otsuka et al.

attractive tensor force decreases spin-orbit splitting of protons with N

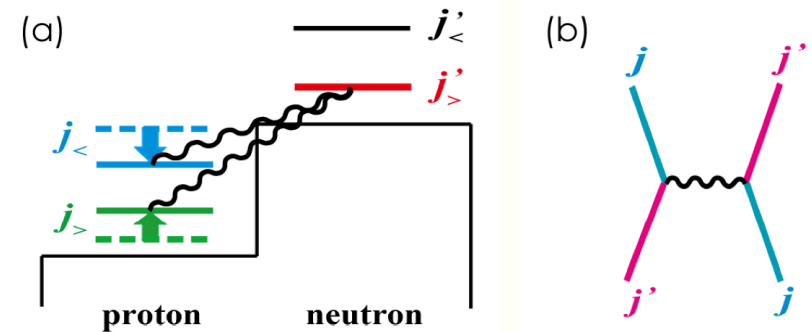
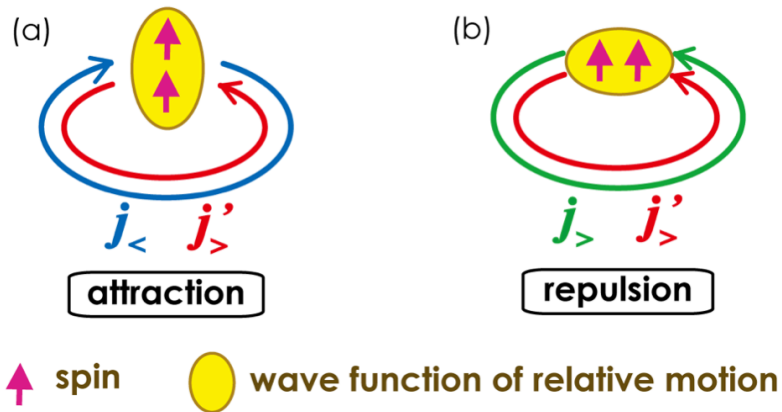
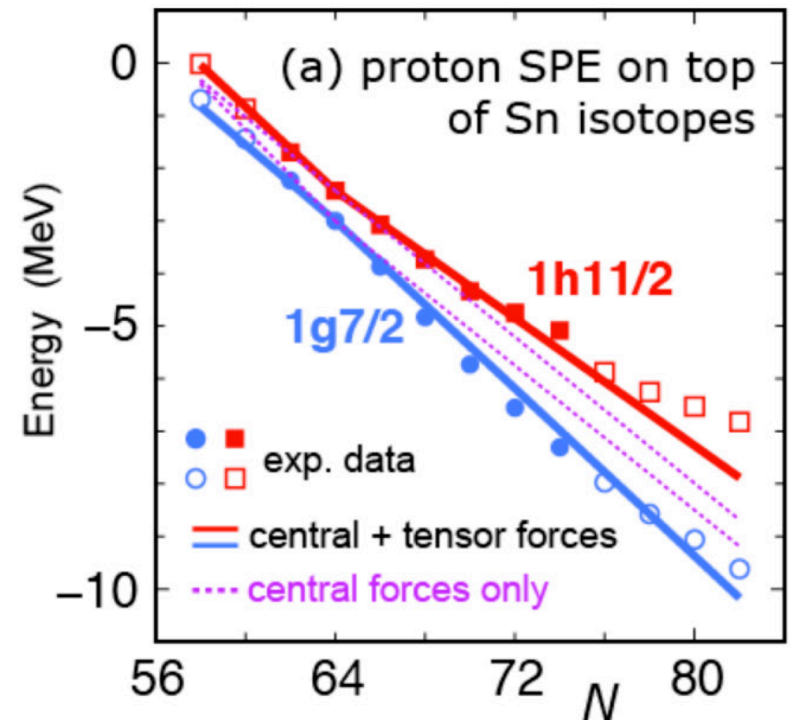


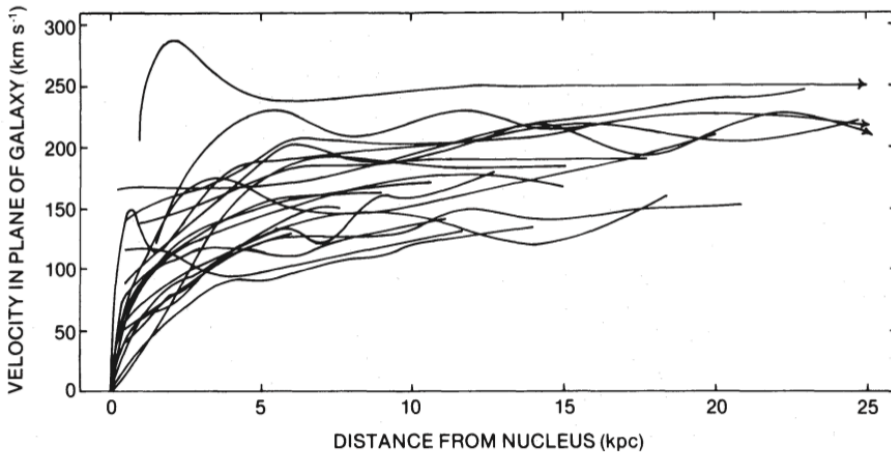
**Figure 2.** (a) Change of spin-orbit splitting by the tensor force. (b) Diagram causing the change in (a). Wavy line stands for the tensor force. Modified from Ref. [6].

larger relative momentum  
decreases horizontal overlap:  
attractive



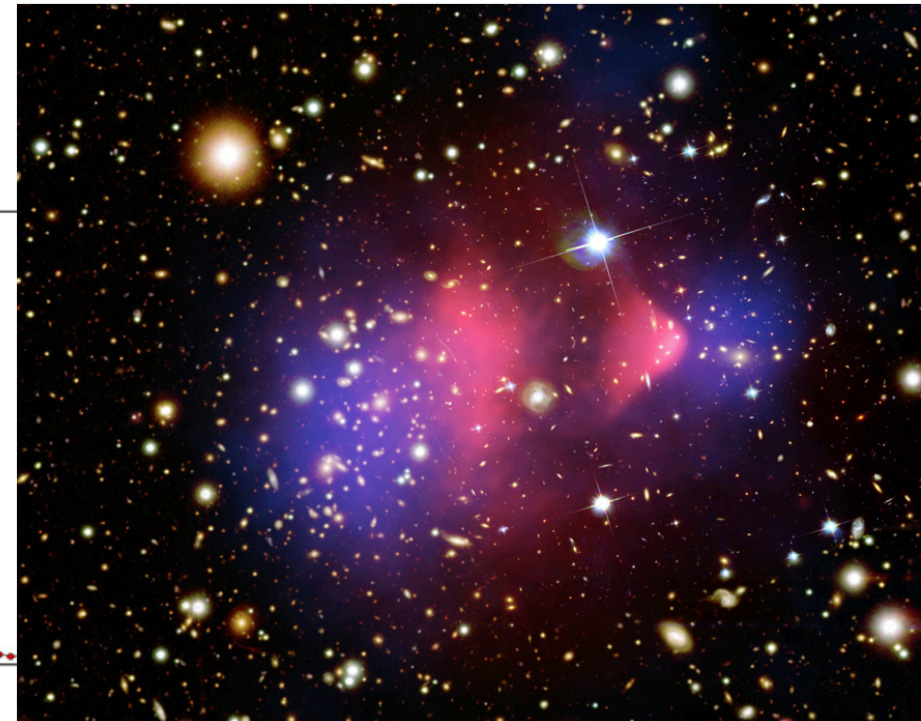
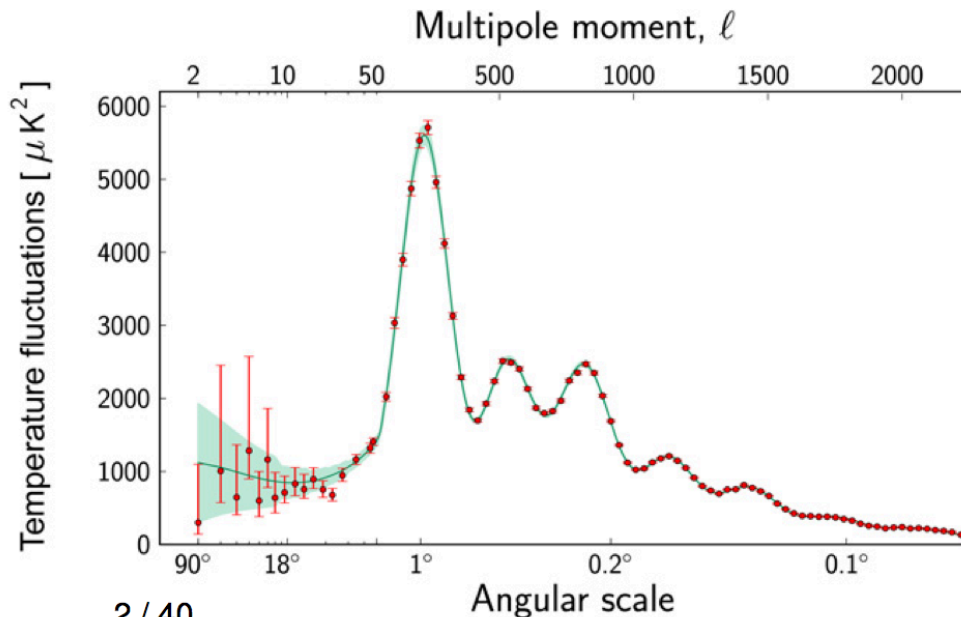


# Dark Matter: evidence



Solid evidence of Dark Matter  
in very different observations:

Rotation curves, Lensing, CMB...  
Zwicky 1930's, Rubin 1970's,..., Planck (2013)



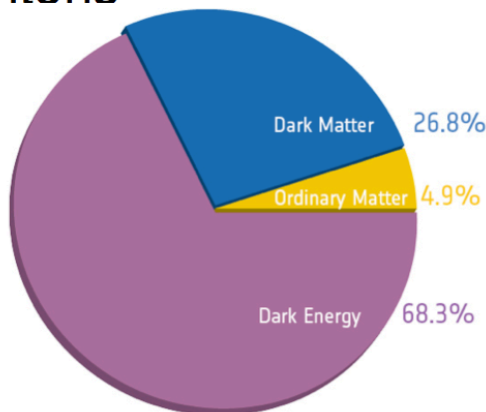
# What is Dark Matter?: WIMPs

We don't know the component of Dark Matter

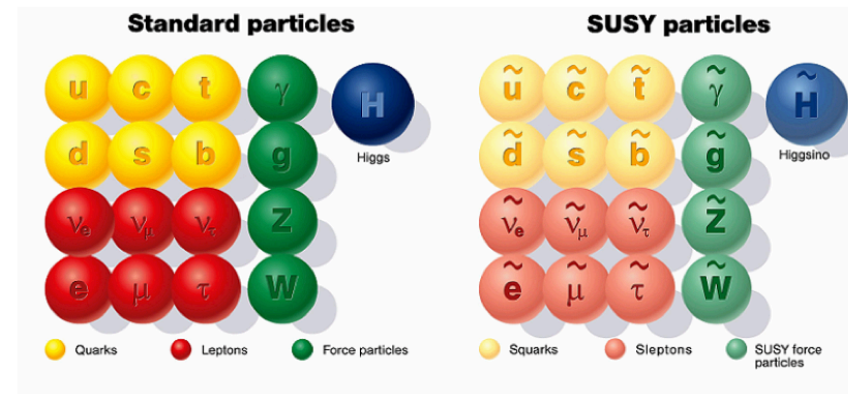
Many very different candidates have been proposed:

New particles: To be detected

- **Weakly interacting massive particles (WIMPs)**
- Sterile neutrinos
- Axions
- Gravitons
- ...



Lightest supersymmetric particles (usually neutralino) predicted in SUSY extensions of the Standard Model



Expected WIMP-density naturally accounts for observed Dark Matter density



# Direct dark matter detection

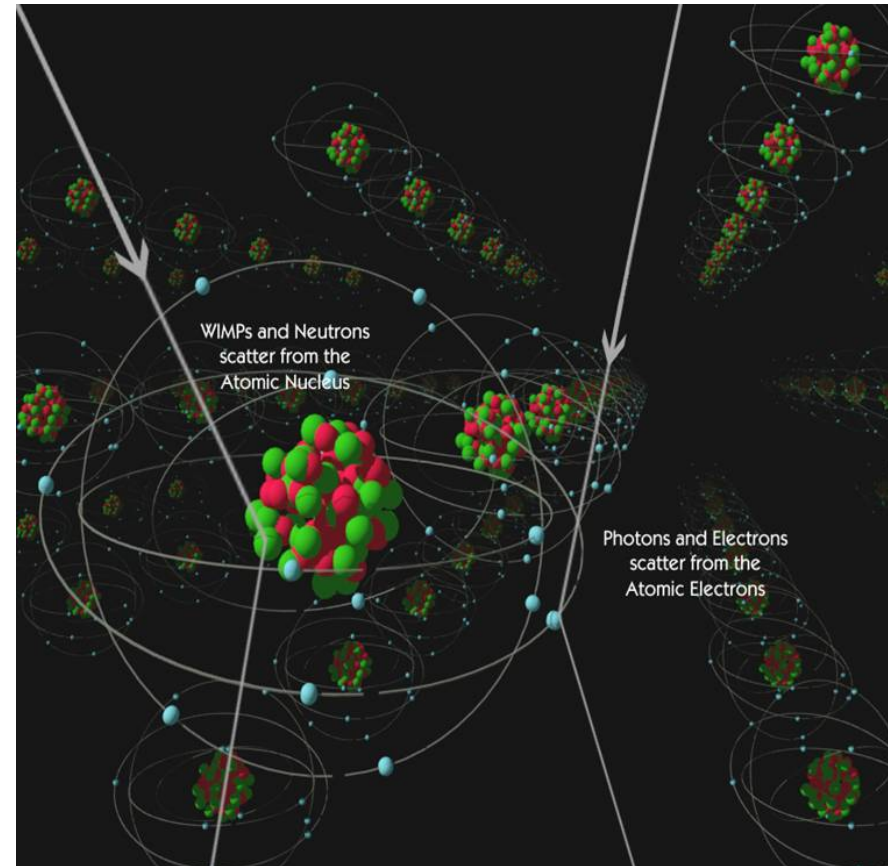
WIMP scattering off nuclei needs **nuclear structure factors** as input  
particularly sensitive to nuclear physics for **spin-dependent** couplings

relevant momentum transfers  $\sim m_\pi$

**calculate systematically**  
**with chiral effective field theory**

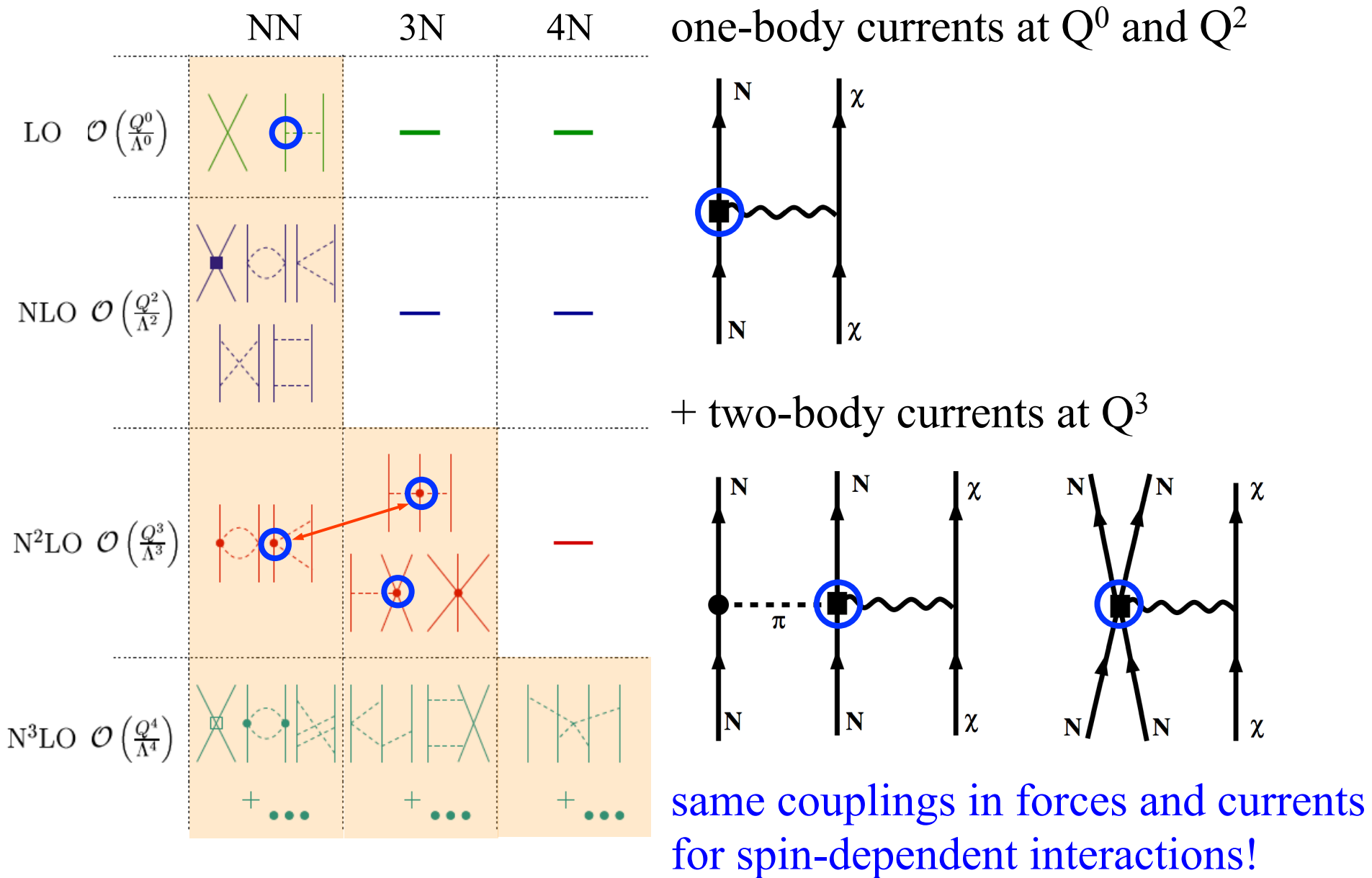
Menendez, Gazit, AS, PRD **86**, 103511 (2012),  
Klos, Menendez, Gazit, AS, 1304.7684.

dark matter response may have  
more complex couplings in nuclei  
Liam Fitzpatrick, Haxton et al. (2012)



from CDMS collaboration

# Chiral EFT for WIMP currents in nuclei

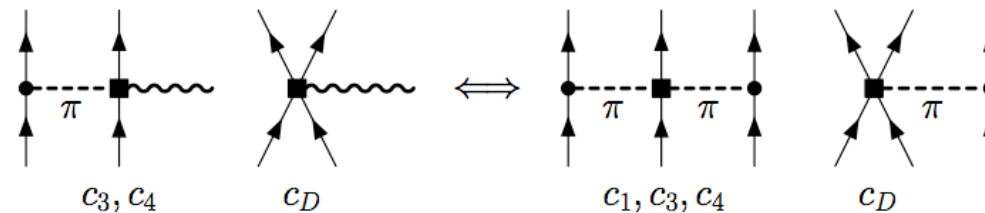


## Two-body currents and 3N forces

weak axial currents and WIMP currents couple to spin, similar to pions  
spin-dep. WIMP-nucleon int. = isospin rotation of weak axial current

two-body currents predicted by  $\pi N$ , NN, 3N couplings to N<sup>3</sup>LO

Park et al., Phillips,...



two-body analogue of Goldberger-Treiman relation

explored in light nuclei, but not for larger systems

dominant contribution to Gamow-Teller transitions,  
important in nuclei ( $Q \sim 100$  MeV)

3N couplings predict quenching of  $g_A$  (dominated by long-range part)  
and predict momentum dependence (weaker quenching for larger  $p$ )

Menendez, Gazit, AS (2011)

# WIMP currents in nuclei and uncertainties

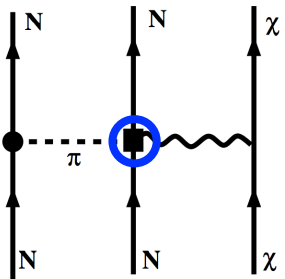
one-body currents with isoscalar/isovector couplings  $a_{0/1}$

$$Q^0 : \sum_{i=1}^A \mathbf{J}_{i,1b} = \sum_{i=1}^A \frac{1}{2} \left[ a_0 \sigma_i + a_1 \tau_i^3 \sigma_i \right]$$

$$Q^2 : \sum_{i=1}^A \mathbf{J}_{i,1b} = \sum_{i=1}^A \frac{1}{2} \left[ a_0 \sigma_i + a_1 \tau_i^3 \left( \frac{g_A(p^2)}{g_A} \sigma_i - \frac{g_P(p^2)}{2mg_A} (\mathbf{p} \cdot \sigma_i) \mathbf{p} \right) \right]$$

$Q^2$  similar to phenomenological currents, but slightly different p-dep.

two-body currents at  $Q^3$  predicted by  $c_3, c_4$  couplings from  $\pi N, NN, 3N$



$$\mathbf{J}_{12}^3 = - \frac{g_A}{4F_\pi^2} \frac{1}{m_\pi^2 + k^2} \left[ 2 \left( c_4 + \frac{1}{4m} \right) \mathbf{k} \times (\boldsymbol{\sigma}_\times \times \mathbf{k}) \tau_\times^3 \right. \\ \left. + 4c_3 \mathbf{k} \cdot (\sigma_1 \tau_1^3 + \sigma_2 \tau_2^3) \mathbf{k} - \frac{i}{m} \mathbf{k} \cdot (\sigma_1 - \sigma_2) \mathbf{q} \tau_\times^3 \right]$$

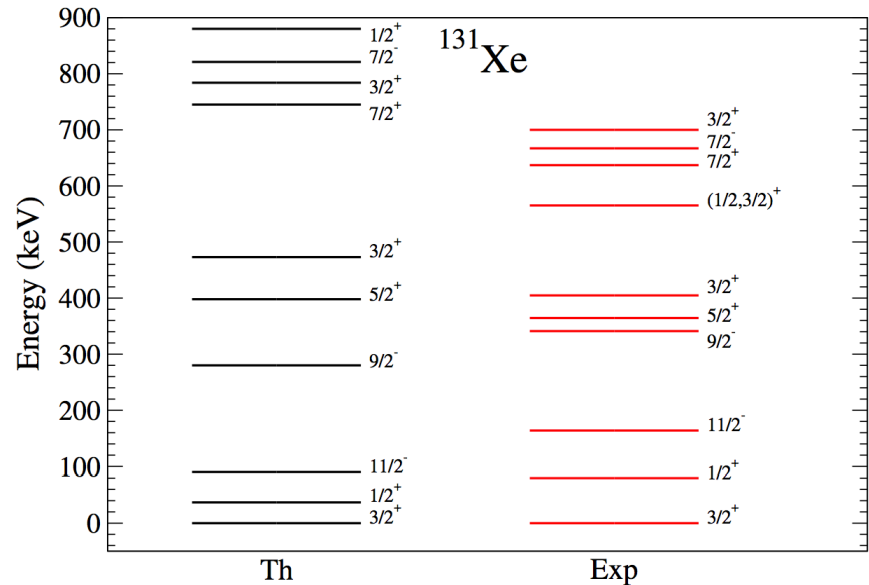
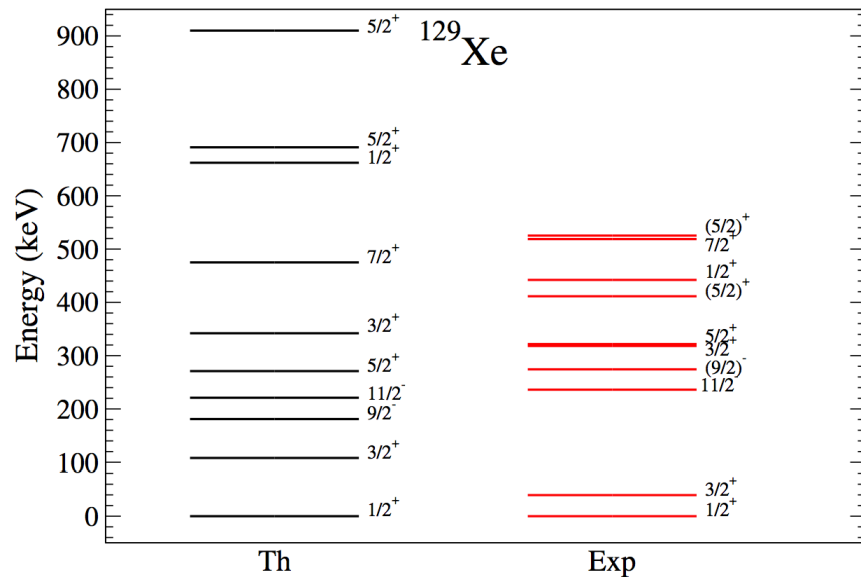
due to interactions among nucleons, dominated by long-range part

include as density-dependent one-body currents (normal ordering),  
uncertainties due to leading-order two-body currents reflected in  $c_3, c_4$

# Nuclear structure for direct detection

valence-shell Hamiltonian calculated from NN interactions + corrections to compensate for not including 3N forces (will improved in the future)

valence spaces and interactions have been tested successfully in nuclear structure calculations, largest spaces used



very good agreement for spectra; ordering and grouping well reproduced

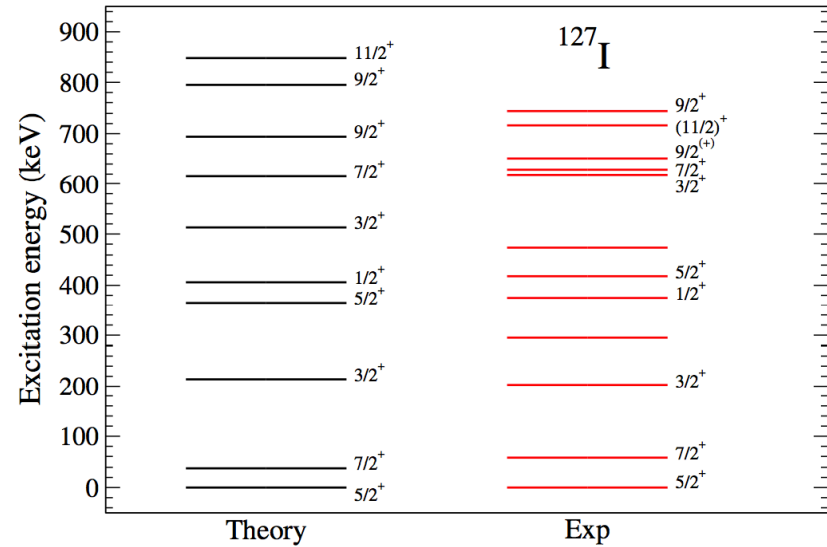
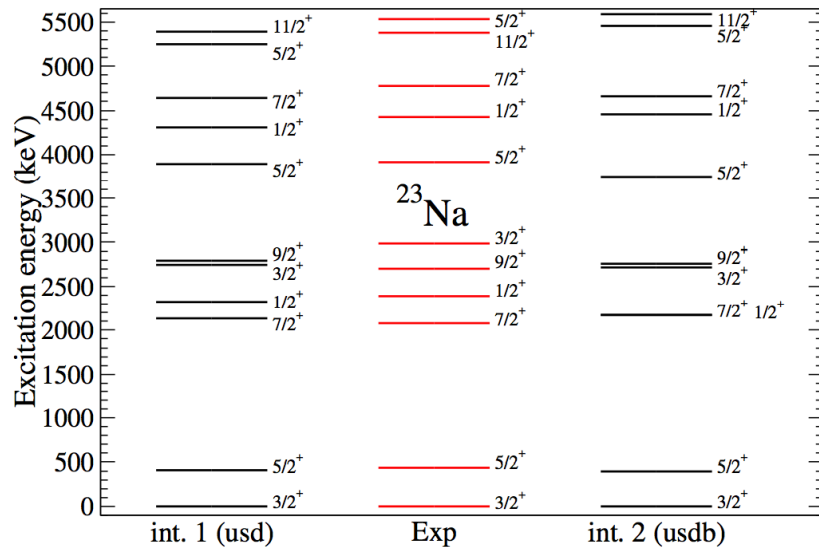
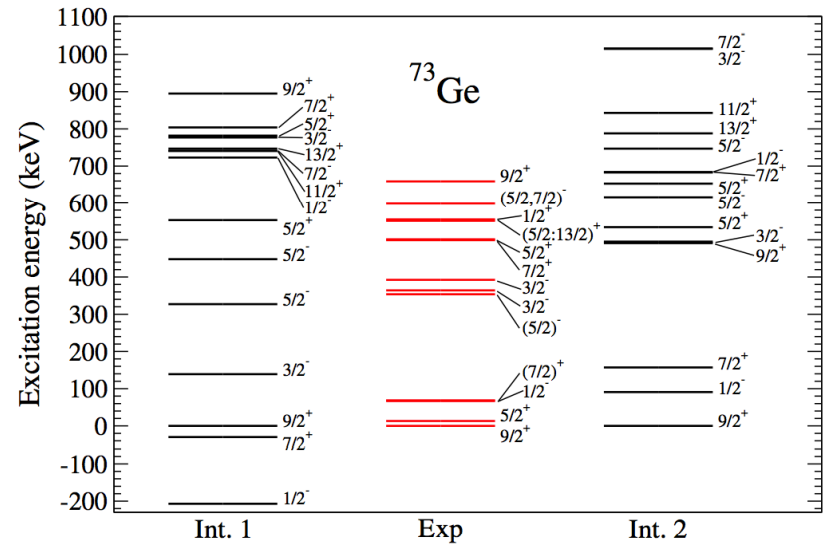
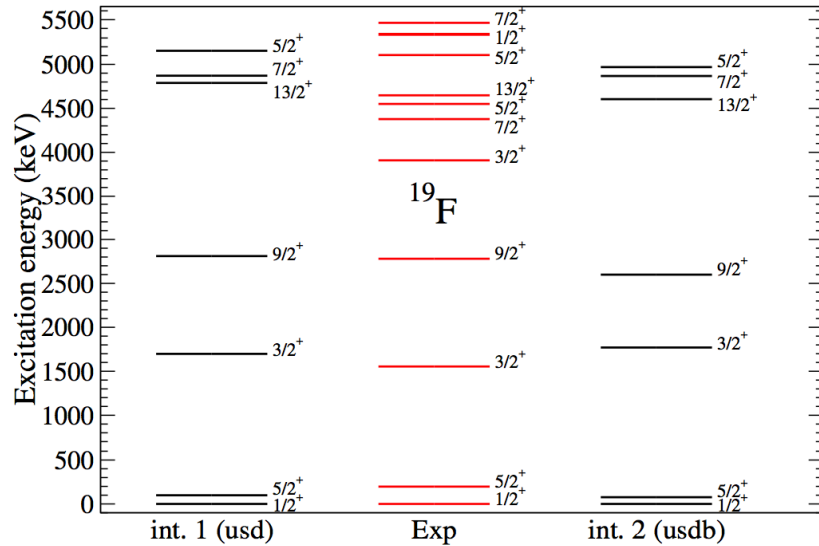
Menendez, Gazit, AS (201)

connects WIMP direct detection with double-beta decay

# Nuclear structure II

similar agreement for other nuclei relevant to direct detection

Menendez, Klos, Gazit, AS (2013)



# Nuclear structure factors

differential cross section for spin-dependent WIMP scattering  
~ axial-vector structure factor  $S_A(p)$

$$\begin{aligned}\frac{d\sigma}{dp^2} &= \frac{1}{(2J_i + 1)\pi v^2} \sum_{s_f, s_i} \sum_{M_f, M_i} |\langle f | \mathcal{L}_\chi^{\text{SD}} | i \rangle|^2 \\ &= \frac{8G_F^2}{(2J_i + 1)v^2} S_A(p),\end{aligned}$$

decompose into longitudinal, transverse electric and transverse magnetic

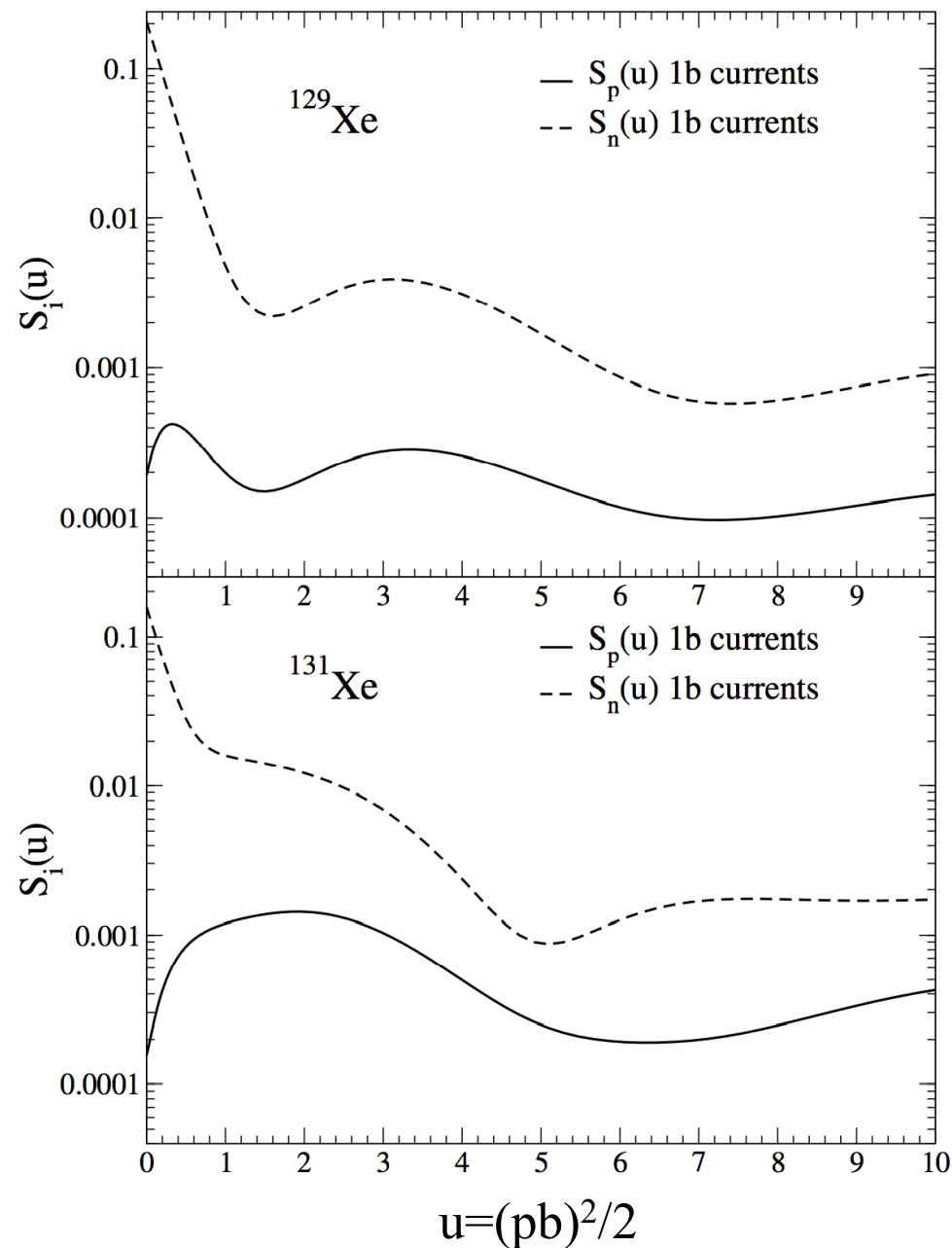
$$\begin{aligned}S_A(p) &= \sum_{L \geq 0} |\langle J_f || \mathcal{L}_L^5 || J_i \rangle|^2 \\ &\quad + \sum_{L \geq 1} \left( |\langle J_f || \mathcal{T}_L^{\text{el}5} || J_i \rangle|^2 + |\langle J_f || \mathcal{T}_L^{\text{mag}5} || J_i \rangle|^2 \right)\end{aligned}$$

transverse magnetic multipoles vanish for elastic scattering

can also decompose into isoscalar/isovector structure factors  $S_{ij}(p)$

$$S_A(p) = a_0^2 S_{00}(p) + a_0 a_1 S_{01}(p) + a_1^2 S_{11}(p)$$

# Xenon response with one-body currents



$^{129,131}\text{Xe}$  are even Z, odd N,  
spin is carried mainly by neutrons

at  $p=0$  structure factors  
at the level of one-body currents  
dominated by “neutron”-only

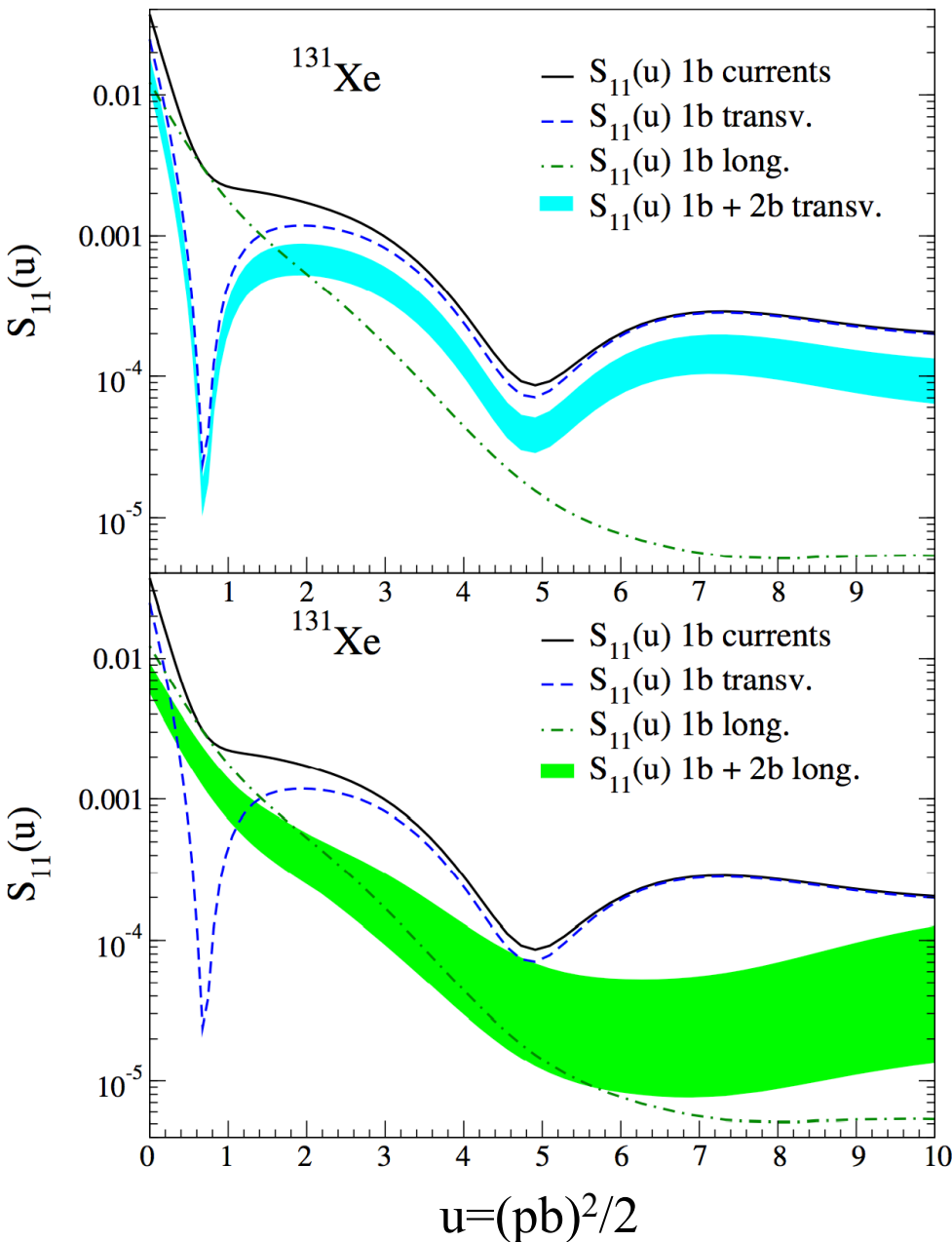
$$S_A = \frac{(2J+1)(J+1)}{\pi J} |a_p \langle S_p \rangle + a_n \langle S_n \rangle|^2,$$

$$a_{n/p} = (a_0 \mp a_1)/2,$$

$$S_n(0) \propto |\langle S_n \rangle|^2 \quad S_p(0) \propto |\langle S_p \rangle|^2.$$



# Xenon response with 1+2-body currents



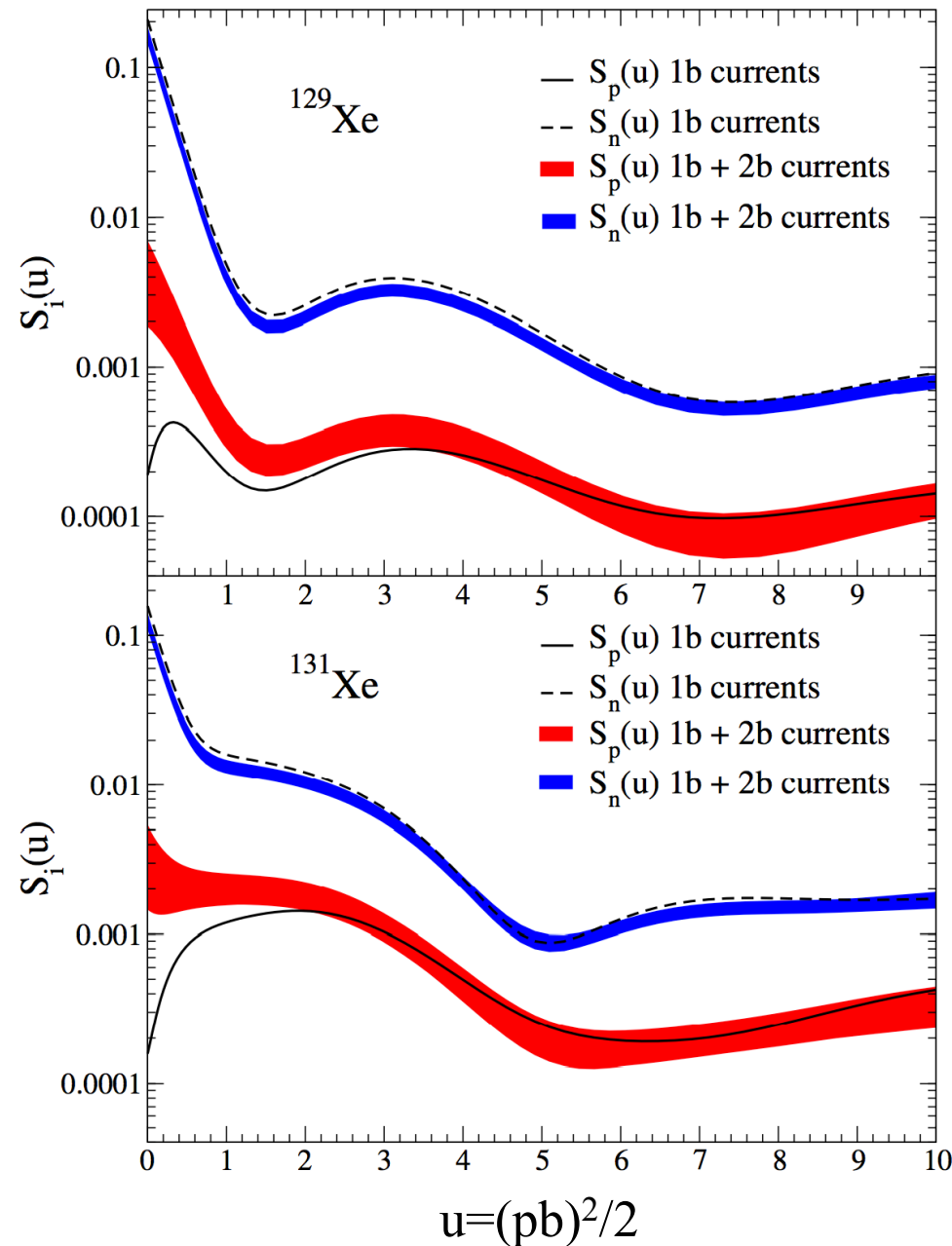
leading two-body currents  
renormalize isovector coupling:  
not “neutron”/“proton” only

lead to reduction of axial current  
enhancement of pseudoscalar curr.

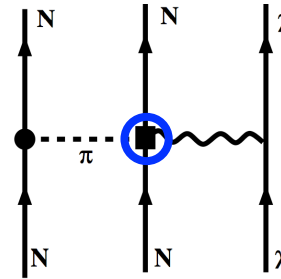
transverse multipoles reduced;  
longitudinal reduced at low  $p$ ,  
but enhanced at high  $p$

uncertainty band due to  $c_3$ ,  $c_4$   
and normal-ordering

# Xenon response with 1+2-body currents



two-body currents due to strong interactions among nucleons



WIMPs couple to neutrons and protons at the same time

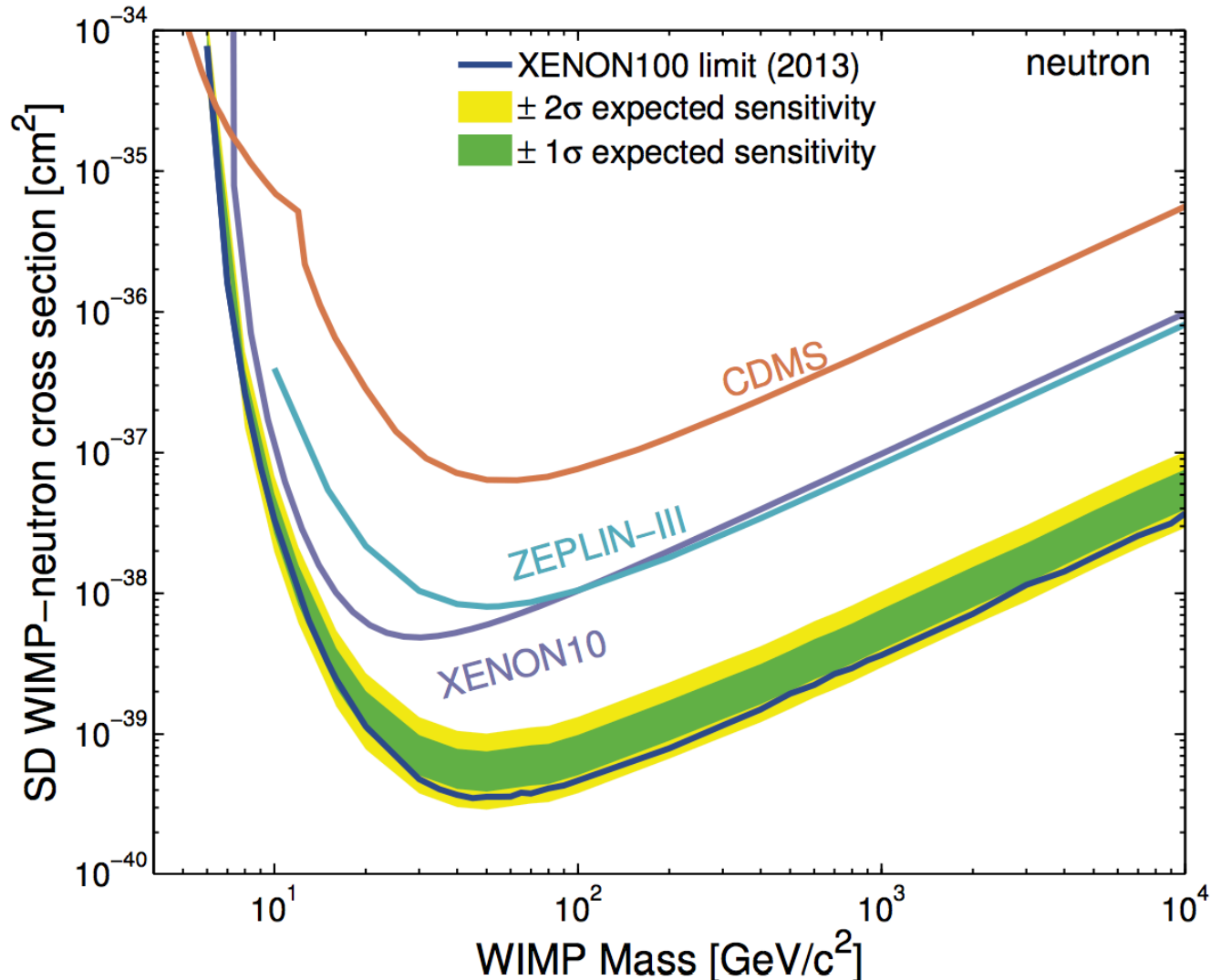
enhances coupling to even species in all cases

first calculations with chiral EFT currents and state-of-the-art nuclear interactions

# Limits on SD WIMP-neutron interactions

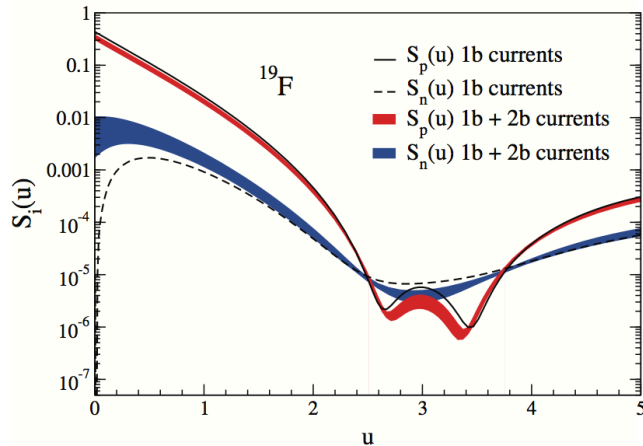
best limits from XENON100 *Aprile et al., PRL (2013)*

used our calculations with uncertainty bands for WIMP currents in nuclei

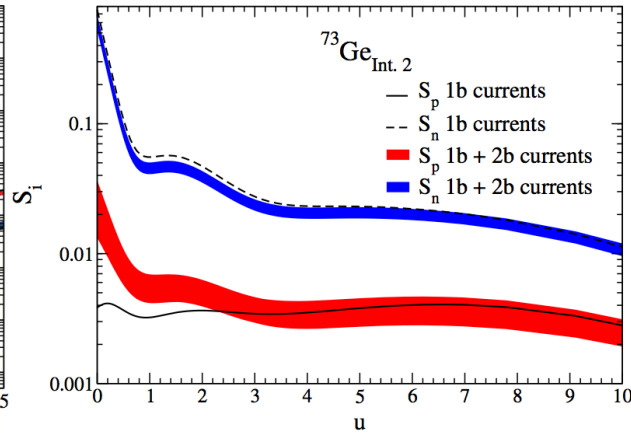


# Spin-dependent WIMP-nucleus response for $^{19}\text{F}$ , $^{23}\text{Na}$ , $^{27}\text{Al}$ , $^{29}\text{Si}$ , $^{73}\text{Ge}$ , $^{127}\text{I}$

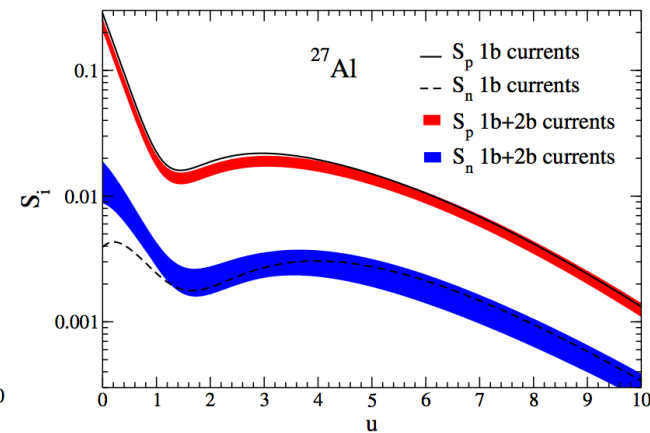
Klos, Menendez, Gazit, AS (2013)



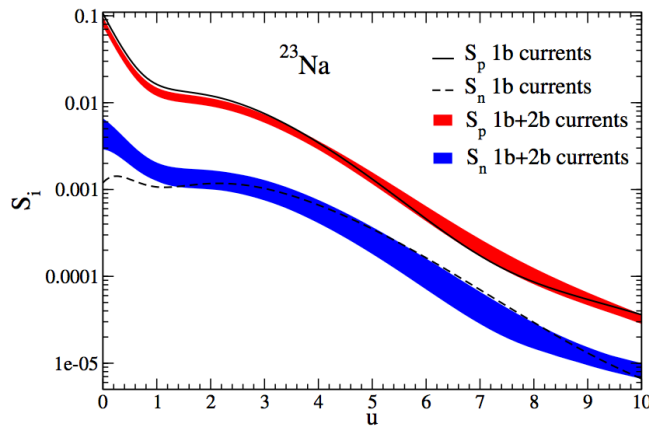
PICASSO, COUPP, SIMPLE



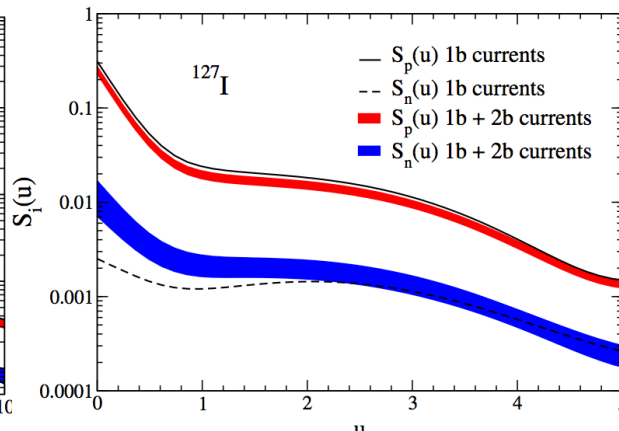
CDMS, EDELWEISS, EURECA



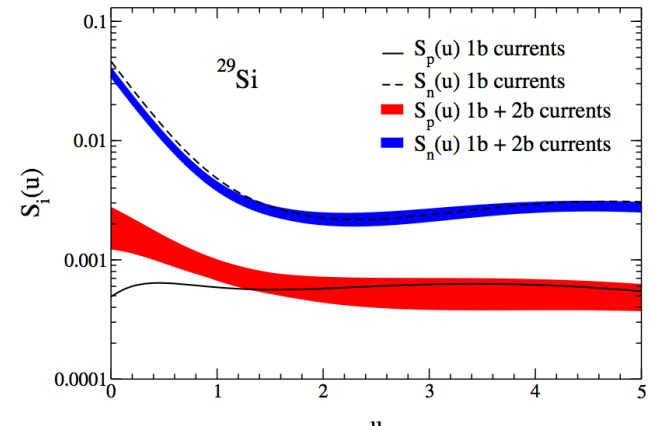
CRESST



DAMA, ANAIS, DM-Ice



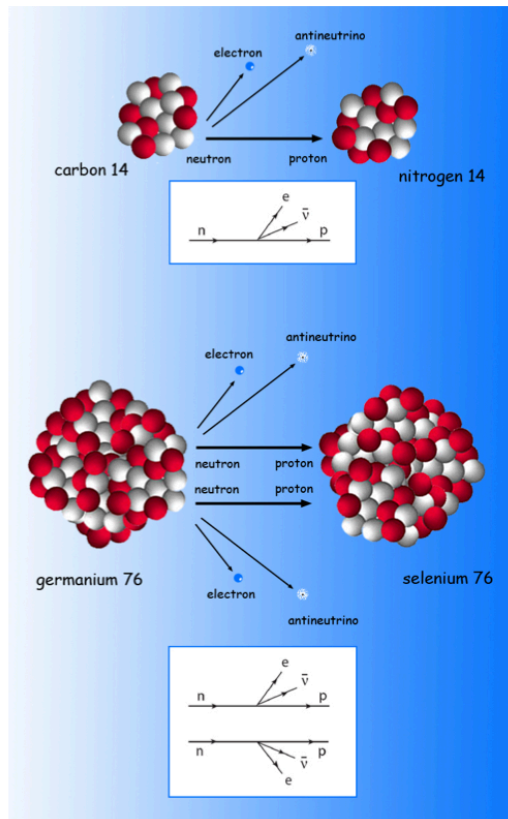
DAMA, ANAIS, DM-Ice, KIMS



CDMS-II

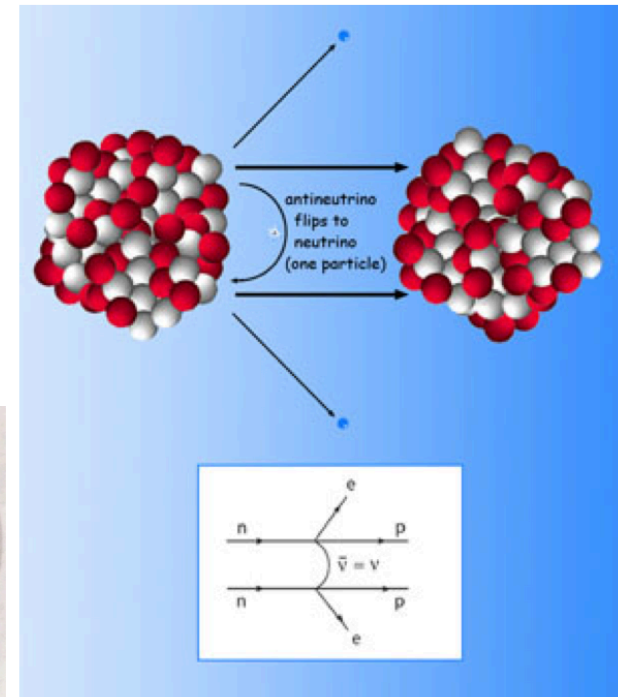
# Neutrinoless Double beta decay

Lepton number conserved in all processes observed so far:



$\beta$  decay,  $\beta\beta$  decay...

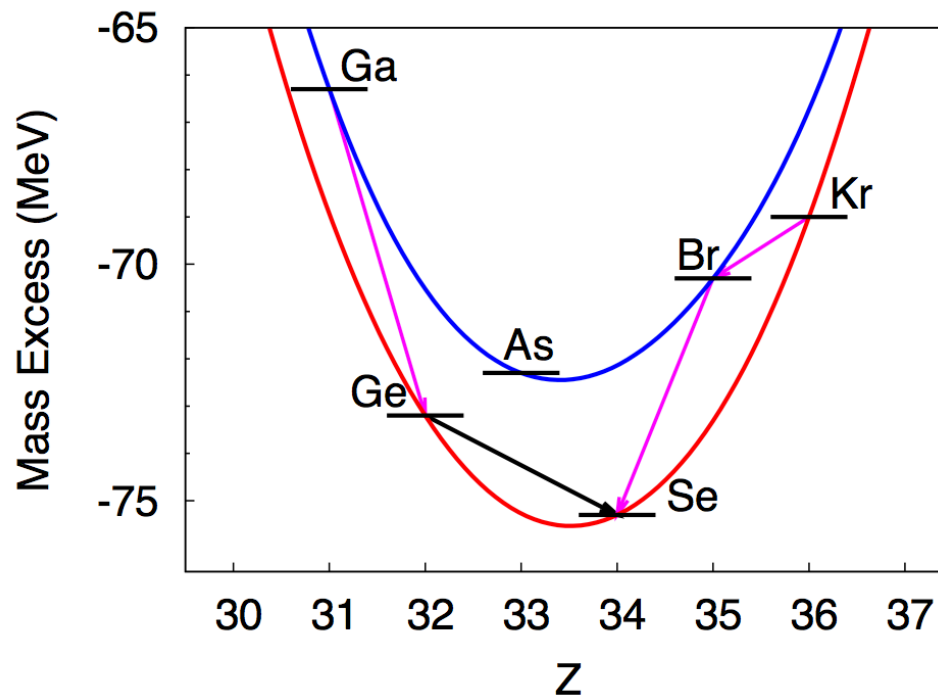
Uncharged massive particles like Majorana neutrinos ( $\nu$ ) theoretically allow L violation



Neutrinoless  $\beta\beta$  ( $0\nu\beta\beta$ ) decay

# Double beta decay: origin

- Double beta decay is a rare second-order weak process
- It only appears when single  $\beta$  decay is energetically forbidden or hindered by large  $J$  difference



# Nuclear Matrix Elements (NMEs)

$0\nu\beta\beta$  process needs massive Majorana neutrinos ( $\nu = \bar{\nu}$ )  
 $\Rightarrow$  detection would proof Majorana nature of neutrinos

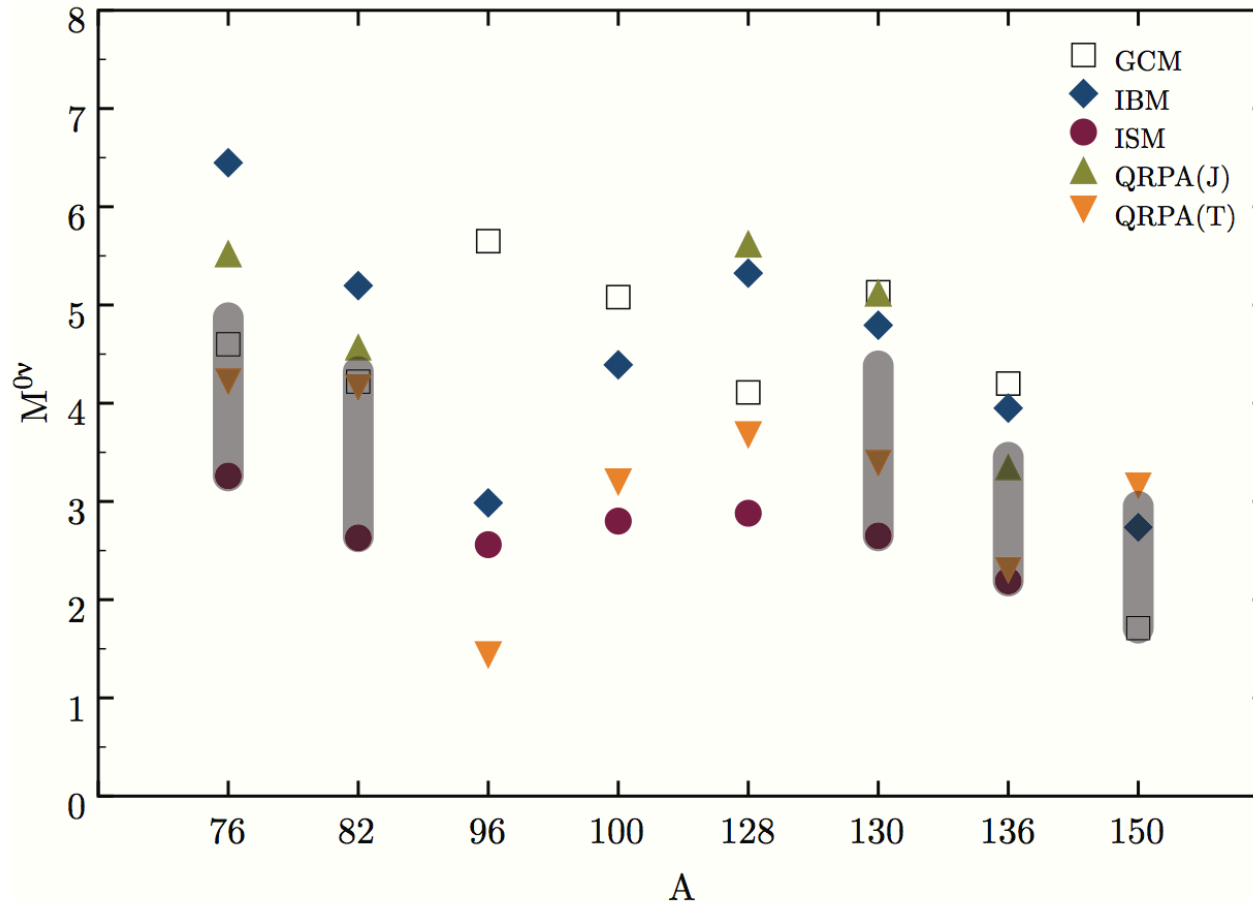
$$\left( T_{1/2}^{0\nu\beta\beta} (0^+ \rightarrow 0^+) \right)^{-1} = G_{01} |M^{0\nu\beta\beta}|^2 \left( \frac{m_{\beta\beta}}{m_e} \right)^2$$

$M^{0\nu\beta\beta}$  necessary to identify best candidates for experiment and to obtain neutrino masses and hierarchy with  $m_{\beta\beta} = \left| \sum_k U_{ek}^2 m_k \right|$

$$M^{0\nu\beta\beta} = \langle 0_f^+ | \sum_{n,m} \tau_n^- \tau_m^- \sum_X H^X(r) \Omega^X | 0_i^+ \rangle$$

- Many-body method to describe initial and final nuclear states (ISM)
- Transition operator, appropriate for this decay (chiral EFT)

# $M^{0\nu\beta\beta}$ uncertainty: nuclear structure



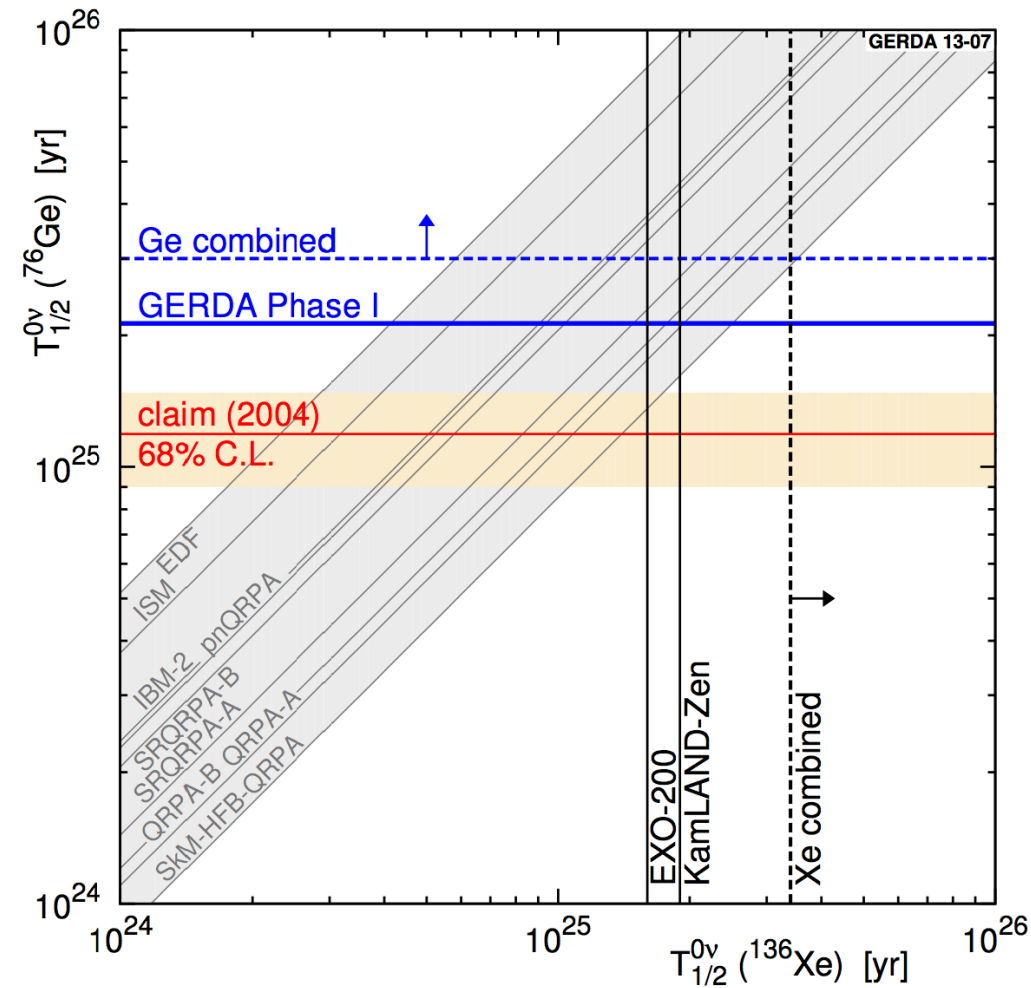
Different calculations  
differ factor  $\sim 2$

Work in progress to:  
improve calculations  
understand  
differences

Gomez-Cadenas et al., JCAP06 007(2011)



# Results from GERDA Phase I Agostini et al., 1307.4720



In conclusion, due to the unprecedented low background counting rate and the good energy resolution intrinsic to HPGe detectors, GERDA establishes after only 21.6 kg·yr exposure the most stringent  $0\nu\beta\beta$  half-life limit for  $^{76}\text{Ge}$ . The long-standing claim for a  $0\nu\beta\beta$  signal in  $^{76}\text{Ge}$  is strongly disfavored, which calls for a further exploration of the degenerate Majorana mass scale. This will be pursued by GERDA Phase II aiming for a sensitivity increased by a factor of about 10.

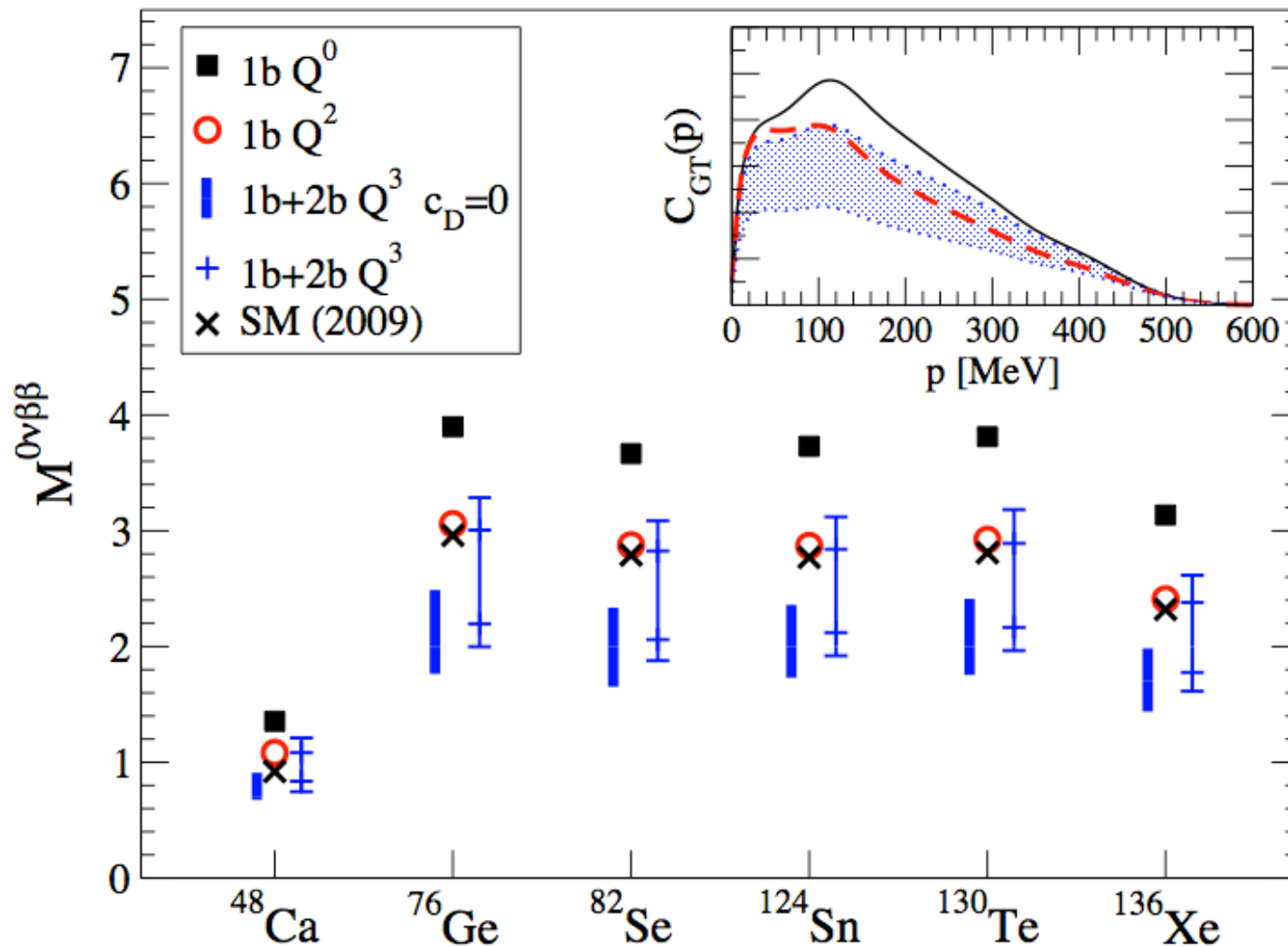
FIG. 2. Limits (90% C.L.) on  $T_{1/2}^{0\nu}$  of  $^{76}\text{Ge}$  (this work) and  $^{136}\text{Xe}$  [14, 15] compared with the signal claim for  $^{76}\text{Ge}$  of Ref. [11] (68% C.L. band). The lines in the shaded gray band are the predictions for the correlation of the half-lives in  $^{136}\text{Xe}$  and in  $^{76}\text{Ge}$  according to different NME calculations [27–33]. The selection of calculations and the labels are taken from Ref. [34].

# Chiral EFT and $0\nu\beta\beta$ decay

Nuclear matrix elements for  $0\nu\beta\beta$  decay based on chiral EFT operator

Menendez, Gazit, AS (2011)

Modest quenching because  $0\nu\beta\beta$  decay probes higher momentum transfer



Thank you for a great 3 weeks!!

